Spectrochimica Acta Part A: Molecular and Biomolecular Spectroscopy 213 (2019) 375–383

Contents lists available at ScienceDirect

Spectrochimica Acta Part A: Molecular and Biomolecular Spectroscopy

journal homepage: www.elsevier.com/locate/saa

Detection of inorganic phosphor in environmental water samples using a lanthanide and nanoparticle chemosensor based on Förster resonance energy transfer

Madeleine Johnson [1], Alaa Fadhel [2], Khang Trieu, Jonathan Daniel, Melanie Beazley, Andres D. Campiglia *

Department of Chemistry, University of Central Florida, P.O. Box 25000, Orlando, FL 32816-2366, USA

ARTICLE INFO

Article history:
Received 12 July 2018
Received in revised form 22 January 2019
Accepted 28 January 2019
Available online 29 January 2019

Keywords:
Inorganic phosphor
Nanosensing assay
FRET
Lanthanide luminescence
Time-resolved luminescence

ABSTRACT

A novel chemosensor is presented for the detection of inorganic phosphate (Pi) in environmental water samples. The sensing solution is comprised of terbium (Tb^{3+}) chelated to ethylenediaminetetraacetic acid (EDTA) acid and cetyltrimethylammonium bromide (CTAB)-capped gold nanoparticles (Au NPs). Upon mixing, Tb-EDTA and Au NPs undergo Förster resonance energy transfer (FRET) in which the luminescence from the lanthanide ion is quenched. Upon the addition of Pi, Au NPs aggregate and precipitate out of solution. The aggregation of Au NPs results in the restoration of the Tb-EDTA luminescence signal, which correlates linearly to the Pi concentration in the matrix of analysis. The limit of detection (LOD) of the luminescence sensor (83 $ng \cdot mL^{-1}$) is within the range of LODs previously reported for on-site monitoring of Pi. Quantitative analysis carried out via the multiple standard additions method provides accurate determination of Pi concentrations in heavily contaminated environmental waters.

© 2019 Published by Elsevier B.V.

1. Introduction

Inorganic phosphate (Pi), also known as orthophosphate, is an essential nutrient for plant growth commonly used in fertilizers. In addition to its agricultural use, Pi finds application in water treatment plants as a pipe corrosion inhibitor [1,2]. While most Pi binds tightly to soils, it does leach into aquatic systems as agricultural run-off over time. This is especially detrimental to closed freshwater bodies where increased Pi concentrations result in algal blooms [3–7]. Algae blooms are often toxic and might lead to eutrophication; a process that reduces the concentration of dissolved oxygen to levels unable to support aquatic life. For instance, the algal blooms and fish kills witnessed along Florida's Treasure Coast in the United States of America during the summer of 2016 are widely regarded as a direct result of the redirection of nutrient-rich agricultural water from Lake Okeechobee into the Banana River [8]. Due to the nature of Pi's gradual release from soils and sediments, it is inherently difficult to predict such eutrophication events by correlating them to times of fertilization. Routine monitoring of water bodies prone to high levels of Pi is therefore needed to predict and prevent eutrophication.

Although numerous analytical methods are capable of detecting Pi at concentrations well below those that would herald an algae outbreak, most approaches are laboratory bound and based on lengthy experimental procedures. This article presents an alternative for the problem at hand, as it proposes a sensing approach with potential for the on-site determination of Pi in water samples. Traditional approaches to Pi detection in aqueous samples are often based on the colorimetric method first reported by Murphy and Riley [9]. In this method, all forms of phosphorous are converted to orthophosphate ions under acid-persulfate digestion. Orthophosphate ions are reacted with ammonium molybdate in acidic solution to form phosphomolybdic acid (PMA); which - in the presence of ascorbic acid and antimony potassium tartrate - is then reduced to phosphoantimonylmolybdenum blue (PAMB). The absorbance of this complex correlates to the concentration of phosphorous ions in the water sample.

In its original form [9], the PAMB method is only able to determine phosphorous ions at the parts-per-million ($\mu g \cdot mL^{-1}$) concentration level; it is prone to chemical interference from barium, lead and silver and/or spectral interference from silicate and arsenate. Preconcentration efforts based on solid-phase [10–12] and liquid-liquid [13,14] extraction have improved the limits of detection (LODs) of the method to parts-per-billion (ppb, $ng \cdot mL^{-1}$) concentration levels. LODs at the ppb level have also been obtained by coupling the PAMB method to ion pairing [15,16] and electrochemical [17–23] approaches.

* Corresponding author.
E-mail address: andres.campiglia@ucf.edu (A.D. Campiglia).
[1] Present address: Integrated Mission Support Services, Kennedy Space Center, FL 32899, USA.
[2] Present address: Al-furat Al-Awsat Technical University - Technical College of Mussaib, Iraq.

https://doi.org/10.1016/j.saa.2019.01.082
1386-1425/© 2019 Published by Elsevier B.V.

Working electrodes specifically tailored to the detection of Pi provide electrochemical methods with added selectivity [22,23]. Specificity of analysis has been also obtained with chromatographic techniques coupled to inductively coupled plasma–mass spectrometry (ICP-MS). The advantages of ICP-MS over PAMB-based methods include shorter analysis times, calibration curves with wider linear dynamic ranges and lower LODs [24–26].

Particularly relevant to the present work are sensing schemes with on-site detection capability for field-monitoring applications [27,28]. Reported chemo-sensors have been based on the photoluminescence properties of quantum dots [29,30] and organic ligands [31] operating on their own or when combined to lanthanide ions such as europium (III) [32–36] and terbium (III) [37,38]. The long-lived emission of the lanthanide ion adds selectivity to the chemo-sensor as it provides the ability to time-resolve short-lived fluorescence from organic matter often encountered in environmental waters.

Herein, we explore the photoluminescence properties of terbium (III) upon Pi interaction with Au NPs. The sensing mechanism is based on the FRET that occurs between the emitting donor (terbium-ethylenediaminetetraacetic acid complex; Tb-EDTA) and the acceptor (Au NPs capped with cetyltrimethylammonium bromide; CTAB). CTAB is an amine based cationic quaternary surfactant often used to avoid aggregation of Au NPs in aqueous solutions via electrostatic repulsion. In the absence of Pi, the luminescence signal of the donor is quenched due to its approximation to the surface of Au NPs. The FRET quenching distance results from hydrophilic and electrostatic interactions between CTAB and negatively charged Tb-EDTA ions. Due to its chemical affinity with CTAB [39–41], the presence of Pi in the sensing solution causes the aggregation of Au NPs and their precipitation out of solution. Since the proximity between donor and acceptor no longer exists, the luminescence signal of Tb-EDTA is restored for the quantitative analysis of Pi.

The first application of this approach was geared towards the analysis of urine samples [42]. Herein, we demonstrate its potential for the analysis of environmental waters with complex chemical composition. The LOD (83 $ng \cdot mL^{-1}$) obtained with the proposed sensor is within the LOD range previously reported for on-site monitoring of Pi [27–38]. The photoluminescence decay of Tb-EDTA provides a direct way to monitor chemical interference in the sample matrix [43]. The simplicity of analysis and the relatively simple instrumentation makes the developed sensor an attractive alternative for the on-site monitoring of environmental waters.

2. Material and methods

2.1. Chemicals and reagents

Nanopure water from a Barnstead Nanopure Infinity water purifier with a resistance of 18 Ω was used throughout. All the reagents and solvents were purchased at their highest available purity and used without further purification. Chloroauric acid ($HauCL_4$) 1% w/v solution was purchased from Medix. EDTA, terbium (III) chloride hexahydrate ($TbCl_3 \cdot 6H_2O$), CTAB, anhydrous trisodium phosphate, and sodium borohydride ($NaBH_4$) were purchased from Sigma Aldrich. Ascorbic acid and chloroform ($CHCl_3$) were purchased from Fisher. 4-(2-Hydroxyethyl)-1-piperazineethanesulfonic acid (HEPES) buffer was obtained from Acros. Nylon syringe filters with a 0.2 μm pore size were purchased from Whatman. Polypropylene filters with a 0.2 μm pore size were purchased from VWR international. Carbon-18 (C18) and silica solid phase extraction (SPE) cartridges were purchased either from Sep-pak or Waters (HLB SPE cartridges).

2.2. Synthesis of Au NPs

Au NPs were synthesized according to a slightly modified seed-mediated growth method originally reported by Nikoobakht and El Sayed [44]. A seed solution was first prepared by adding 1 mL of 0.2 M CTAB solution and 1 mL of 0.0005 M $HAuCl_4$ to a 10 mL beaker. The beaker was gently heated (30 °C) on a hot plate to keep the CTAB from precipitating out of solution. A 60 μL volume of ice cold $NaBH_4$ was added to the beaker and stirred gently until the seed solution changed colors from yellow to brown. A growth solution was prepared by heating gently a mixture of 5 μL of 0.2 M CTAB and 5 mL of 0.001 M $HAuCl_4$ in a 10 mL beaker. To this solution, 70 μL of freshly prepared 0.788 M ascorbic acid were added and stirred manually causing the solution to change colors from bright yellow to clear. Still under heating, 15 μL of the seed solution were transferred to the clear solution and stirred manually for 10 s. The mixture was left to sit for about 15–20 min, time during which the solution changed colors from clear to deep purple. The purple solution was removed from the hot plate and stored for later use. Centrifugation was used to remove the excess of CTAB. Prior to centrifugation, the Au NPs solution was gently heated to dissolve the precipitated CTAB. 1 mL aliquots of the Au NPs homogeneous solution were then added to 1.5 mL centrifuge tubes and centrifuged at 13,400 rpm for three 20 min cycles. After the 1st centrifugation cycle, 800 μL of the supernatant were replaced with 800 μL of nanopure H_2O. After 2nd cycle, 900 μL of the supernatant were replaced with 900 μL of nanopure H_2O and, after the 3rd cycle, 900 μL of supernatant were replaced with 450 μL of nanopure H_2O.

2.3. Characterization of Au NPs

The centrifuged solutions of Au NPs were analyzed via UV–vis absorption spectroscopy by mixing 250 μL of 2.5 mM HEPES buffer with 250 μL of centrifuged Au NPs. The particle size distribution of Au NPs was monitored via light scattering measurements using a Zetasizer Nano ZS9 instrument purchased from Malvern. The synthetized nanoparticles were stable at room temperature and could be stored for several months without aggregating.

2.4. Filtration of water samples

Each filtration was performed by drawing 10 mL of water sample into a plastic syringe. The water was then passed through either a nylon or polypropylene syringe filter and collected into a clean vial for further use.

2.5. Liquid-liquid extraction (LLE) of water samples

5 mL of the filtered water sample was mixed with 5 mL of chloroform ($CHCl_3$) and mixed vigorously in a separation funnel. Once the layers had settled, the bottom layer was discarded and the aqueous layer collected into a clean vial for further use.

2.6. Solid-phase extraction (SPE) of water samples

Solid-phase extractions were carried out with the help of a glass block SPE vacuum manifold consisting of polypropylene test tube racks, a bleed valve, and a vacuum control valve. The vacuum rate was adjusted to 12–13 mm Hg for conditioning and extraction. Each cartridge was conditioned with 5 mL of methanol followed by 10 mL of nanopure water. A 5 mL volume of water sample was processed through the cartridge and the eluent was collected for photoluminescence spectroscopy.

2.7. Analysis of environmental waters

Three water samples of known Pi concentration were analyzed with the developed sensor. Two of the studied samples - namely 06A and 07A - were obtained from Florida Spectrum Environmental Services. Both samples consisted of agricultural waters with relatively high concentrations of Pi. According to ion chromatography (IC) and potentiometric data provided by Florida Spectrum Environmental Services, the water

sample 06A had the following anion composition: 131.2 $\mu g \cdot mL^{-1}$ fluoride, 360.2 $\mu g \cdot mL^{-1}$ chloride, 146.8 $\mu g \cdot mL^{-1}$ sulfate, and 125.1 $\mu g \cdot mL^{-1}$ Pi. The anion composition of sample 07A was as follows: 946.9 $\mu g \cdot mL^{-1}$ chloride, 245.5 $\mu g \cdot mL^{-1}$ sulfate and 1548 $\mu g \cdot mL^{-1}$ Pi. These IC data was obtained with an 881 Compact IC Pro (Metrohm AG) instrument. Filtered samples were separated on a MetroSep A Supp anion exchange column using carbonate/bicarbonate eluent and suppressed conductivity detection with an LOD for orthophosphate (PO_4^{3-}) of 0.080 mg L^{-1}.

The third sample was an untreated wastewater sample collected from influent at the Iron Bridge Water Pollution Control Facility, located in the City of Orlando, Florida. The wastewater sample – which is referred to as BWW – contained the following anion concentrations as determined by ion chromatography: 75.3 $\mu g \cdot mL^{-1}$ chloride, 1.86 $\mu g \cdot mL^{-1}$ sulfate, and 10.4 $\mu g \cdot mL^{-1}$ phosphate. Anion concentrations were obtained by IC with the aid of a Dionex ICS-1100 series integrated IC system (Thermo Fisher Scientific). Filtered samples were separated on a Dionex Ion Pac AS23 anion exchange column using carbonate/bicarbonate eluent and suppressed conductivity detection. The LOD for orthophosphate was 0.10 mg L^{-1}.

Due to their rather large Pi concentrations and the possibility of sensor saturation, sample 06A and 07A were diluted with nanopure water by a factor of 5 and 3, respectively. Sample BWW was analyzed as received. All water samples analyzed with the Pi sensor were submitted to filtration and LLE as previously described.

2.8. UV–vis absorption spectroscopy

Absorbance measurements were made with a double-beam Cary 50 spectrometer equipped with a 75-W pulsed Xenon lamp (spectral radiance from 190 to 1100 nm), a monochromator with a 24,000 nm/min maximum scan rate and 1.5-nm fixed optical band-pass, a beam-splitter and two silicon photodiode detectors.

2.9. Photoluminescence spectroscopy

Photoluminescence measurements were made with a commercial spectrofluorimeter (Photon Technologies International) using microliter volume quartz cuvettes. All measurements were carried out at a 90° configuration. No sample de-oxygenation was attempted. For steady state (SS) measurements, the excitation source was a continuous wave 75 W Xenon lamp with broadband illumination from 200 nm to 1000 nm. Detection was made with a photomultiplier tube with wavelength range from 185 to 650 nm. For time-resolved (TR) measurements in the milliseconds time domain, the excitation source was a pulsed 75 W Xenon lamp (wavelength range from 200 to 2000 nm), variable repetition rate from 0 to 100 pulses per second, and a pulse width of approximately 3 μs. Detection was made with a gated analog photomultiplier tube (PMT, Model 1527). Its spectral response extended from 185 to 900 nm. SS and TR spectra were recorded with excitation and emission monochromators having the same reciprocal linear dispersion (4 $nm \cdot mm^{-1}$) and accuracy (±1 nm with 0.25 nm resolution). Their 1200 grooves/mm gratings were blazed at 300 and 400 nm, respectively. The instrument was computer controlled using commercial software specifically designed for the system.

3. Results and discussion

3.1. Characterization of Au NPs

The batch-to-batch reproducibility of the synthetic procedure was monitored via UV–vis spectroscopy and light scattering measurements. Typical examples of UV–vis absorption spectra and size distribution data recorded from synthetized batches of Au NPs are shown in Fig. S1. Each batch of Au NPs had an approximate optical density of 1.5 AU (absorbance units) and a single SPR peak of maximum absorption wavelength approximately equal to 532 nm. The presence of only one SPR peak is an indicative of the spherical shape of the synthetized NPs. The size distribution of the spherical NPs was found to be in the range of 52 nm, which is consistent with the observed SPR peak at 532 nm [44,45].

3.2. Photoluminescence probe

Since Pi detection relies on the release of Tb^{3+} into the sample matrix, the LOD of the proposed sensor depends on the ability to measuring low concentrations of the lanthanide ion in water samples. The long-lived photoluminescence signal of Tb^{3+} allows to time-resolve short-lived background fluorescence and scattered radiation light from complex matrixes with relatively simple commercial instrumentation [46,47]. Because its emission involves shielded f-level electronic transitions, the intensity of its luminescence signal is less sensitive to oxygen quenching than traditional fluorescence dyes. Counterbalancing these advantages is the low intensity of the photoluminescence signal of T^{b3+} in aqueous media. Upon binding to the lanthanide ion, water molecules quench its luminescence via weak vibronic coupling with the vibrational states of the O—H oscillators [48]. Adequate intensities for analytical use are often obtained with the aid of chelating agents that remove water molecules from the primary coordination of Tb^{3+}. Because the emission of the chelated ion remains in the microsecond to milliseconds time domain, discrimination of fluorescence background and light scattering is still possible with conventional pulsed sources readily available in commercial instrumentation.

Upon interaction with $EDTA^{4-}$, the maximum luminescence signal of Tb^{3+} is obtained at a 1:1 $EDTA^{-4}$:Tb^{3+} molar. At this molar ratio, $EDTA^{4-}$ occupies six sites in the first coordination sphere of Tb^{3+}, which leaves 3 additional sites available for chemical interaction with the surrounding medium [42]. A delay time of 250 μs was sufficient to time discriminate the fluorescence background of the 25 mM HEPES solution. A gate time of 9 ms provided the best signal to background ratio under a reasonable time for spectral acquisition. An integration time of 500 μs was found to be optimal for signal measurements. Longer integration times did not yield any further luminescence enhancements. Since a 10^{-4} M Tb-EDTA solution provided an acceptable spectral signature for analytical use, all sensing measurements were then performed with this chelate concentration at excitation/emission wavelengths of 248/548 nm and delay/gate/integration times of 250 μs/9 ms/500 μs.

3.3. Quenching Effect of Au NPs

The aggregation of Au NPs caused by the presence of Pi in the sensing solution displaces Tb-EDTA from the proximities of Au NPs to the extent that FRET does no longer occur. The time it takes for the signal of the donor to reach its maximum intensity depends on the concentration of Pi in the water sample and the shaking time after mixing the water sample with the sensing solution. For the range of Pi concentrations tested, the longest (15 min) and the shortest (5 min) times were observed with 190 $ng \cdot mL^{-1}$ and 332 $ng \cdot mL^{-1}$ Pi solutions, respectively. In order to provide enough time for the complete displacement of Tb-EDTA, all further measurements were then made after 15 min of shaking time at 1000 rpm.

3.4. Sensing solution

The volume of the Au NPs solution needed to reach the maximum quenching of the Tb-EDTA signal depends on the volume and the concentration of the donor solution added to the sensing solution. For 50 μL of a 10^{-4} M Tb-EDTA, maximum quenching of the luminescence signal was observed with 250 μL of an Au NPs solution with optical density = 1.50 AU. Since 200 μL of 2.5 mM HEPES buffer was found to have ample buffering capacity to hold the pH at ~7.4 upon addition of microliter volumes of environmental water samples, the sensing solution for

Table 1
Analytical figures of merit for the analysis of Pi in nanopure water.

$\lambda_{exc}/\lambda_{em}$[a] (nm)	$t_d/t_g/t_i$[b] (ms)	LDR[c] (ppb)	R[d]	y = mx + b[e]	s_R[f] (cps)	LOQ[g] (ppb)	LOD[h] (ppb)
248/548	250/9000/500	130–332	0.9860	2.11x + 210.9	27.4	130	39

[a] $\lambda_{exc}/\lambda_{em}$ = excitation and emission wavelengths used to measuring signal intensities.
[b] t_d = delay time; t_g = gate time; and t_i = integration time.
[c] LDR = linear dynamic range of the calibration curve.
[d] R = correlation coefficient.
[e] y = mx + b = the best linear fitting obtained via the least squares method, where m = slope and b = intercept.
[f] s_R = standard deviation of the reference signal of the sensor based on 16 determinations of the blank signal.
[g] LOQ = limit of quantitation = $10s_R$ / m.
[h] LOD = limit of detection = $3s_R$ / m.

all further studies was comprised of 50 μL of a 10^{-4} M Tb-EDTA, 250 μL of Au NPs solution with optical density 1.5 AU and 200 μL of 2.5 mM HEPES buffer prepared in nanopure water.

3.5. Limit of quantitation and limit of detection

Table 1 summarizes the analytical figures of merit of the proposed sensor. The calibration curve was built with external standards consisting of pure Pi solutions prepared in HEPES buffer (pH ≈ 7.4). Each data point plotted in the calibration graph corresponded to the average intensity of single measurements made from three sensing solutions mixed with Pi standards. No efforts were made to experimentally determine the upper concentration limit of the linear dynamic range. The lower concentration limit corresponds to the limit of quantitation (LOQ = 130 ng·mL^{-1}) calculated as $10s_R$/m; where s_R is the standard deviation of the sensor in the absence of Pi (reference signal) and m is the slope of the linear plot obtained with the least squares method. The limit of detection (LOD = 39 ng·mL^{-1}) was calculated as $3s_R$ / m. According to previously reported data [30,49,50], these levels of detection are adequate for the analysis of Pi in environmental water samples.

3.6. Filtration of water samples

Prior to Pi analysis, water samples 06A, 07A and BBW were filtered to remove the presence of suspended solids. Solid particulate is known to interfere with optical measurements due to scattering of excitation and/or emitted radiation. Two types of filters were investigated for the purpose at hand; namely nylon and propylene filters. Both types of filters showed equivalent capabilities for removing particulate matter.

Possible Pi losses due to filtration were investigated by monitoring the aggregation of Au NPs as a function of Pi concentration in the eluent of a filtered Pi standard solution. As shown in Fig. S2, the addition of Pi to a solution of Au NPs causes a red shift in the maximum SPR wavelength of the Au NPs as well as a reduction in the optical density of the solution. The red shift can be attributed to the gold nanoparticles aggregating to form conglomerates with a larger diameter and therefore a longer SPR wavelength. The reduction in optical density can be attributed to aggregates precipitating out of solution once they reach a size that is too large for them to remain suspended in water.

Filtration experiments were conducted with a 1147 μg·mL^{-1} Pi standard solution prepared in 2.5 mM HEPES. 10 mL of the standard solution were filtrated and 10 μL of the filtrate were added to 500 μL of an Au NPs solution (optical density = 1.5 AU) prepared in 2.5 mM HEPES. The final mixture was shaken for 15 min at 1000 rpm and its absorbance was measured immediately after shaking. The absorption spectra recorded from the filtrates were then compared to the absorption spectrum recorded from a "control solution" consisting of 10 μL of 1147 μg·mL^{-1} Pi and 500 μL of Au NPs (optical density = 1.5 AU) prepared in 2.5 mM HEPES. This procedure was repeated three times with three 10 mL aliquots of 1147 μg·mL^{-1} Pi standard for each type of investigated filter. The obtained results are shown in Fig. S3-A and -B.

Comparison of the maximum SPR wavelengths in Fig. S3-A indicates that the Pi solution that was passed through the nylon filters did not cause as much aggregation of Au NPs as the control (unfiltered) Pi solution did. This is an indication that nylon retains some of the Pi and decreases its concentration in the filtrated solution. On the other end, Fig. 3S-B shows similar redshifts of SPR maximum wavelengths for filtered and unfiltered (control) Pi standard solutions. This is an indication that polypropylene does not retain Pi to the same extent that nylon does. The observed difference is likely due to the largely alkaline nature of the polypropylene polymer, which does not have any hydrogen bond accepting or donating functional groups. Nylon filters consist of amide bonds which, like Pi, are capable of hydrogen bonding. The lone pairs on the nitrogen and oxygen components of the polymer chain act as hydrogen bond acceptors while the hydrogen attached to the nitrogen acts a hydrogen bond donor. The Pi standard solutions were made in 2.5 mM HEPES buffer and therefore have a pH of about 7.4; at this pH the dominant Pi species is $H_2PO_4^-$, an anion with accepting and donating hydrogen bonding capability. It can therefore be assumed that some Pi is retained in the nylon filter due to hydrogen-bonding interaction.

Table 2
Effect of inorganic ions to the photoluminescence intensity of the probe.

10^{-4} M Tb-EDTA^{-1}	Signal intensity[a] (cps)	t_{exp}[b]
2.5 mM HEPES buffer	1324 ± 14	–
500 ppm PO_4^{3-}	1268 ± 24	3.49
250 ppm SO_4^{2-}	1281 ± 10	4.32
900 ppm Cl^-	1278 ± 6	5.23
250 ppm SO_4^{2-} + 900 ppm Cl^-	1271 ± 10	5.33
500 ppm PO_4^{3-} + 250 ppm SO_4^{2-} + 900 ppm Cl^-	1280 ± 5	5.13

[a] Reported values are the average of three signal intensity measurements performed from three aliquot samples. Excitation and emission band-pass = 4 and 3 nm, respectively.
[b] Experimental value of t obtained from significance test (P = 95%) comparing the signal intensity of the sensor in the absence (npH_2O) and the presence of inorganic ion. $t_{exp} \geq t_{crit} = 2.776$ indicates statistical difference in the absence or presence of the inorganic ion.

Table 3
Effect of environmental waters[a] on the photoluminescence properties of the FRET sensor.

Water sample[a]	Lifetime (ms)[b]	t_{exp}[c]	Intensity (cps)[b]	t_{exp}[c]
06A	601 ± 23	26.4	643 ± 13	61.7
07A	914 ± 20	15.1	807 ± 43	19.8
BWW	1213 ± 59	2.187	1106 ± 21	15.0

[a] Untreated water sample.
[b] Average of three measurements made from individual water samples. Excitation and emission band-pass = 4 and 3 nm, respectively.
[c] Experimental value of t calculated from the averages and standard deviations from the previous column and the control. $t_{exp} \leq t_{crit} = 2.776$ indicates statistical equivalence with the control.

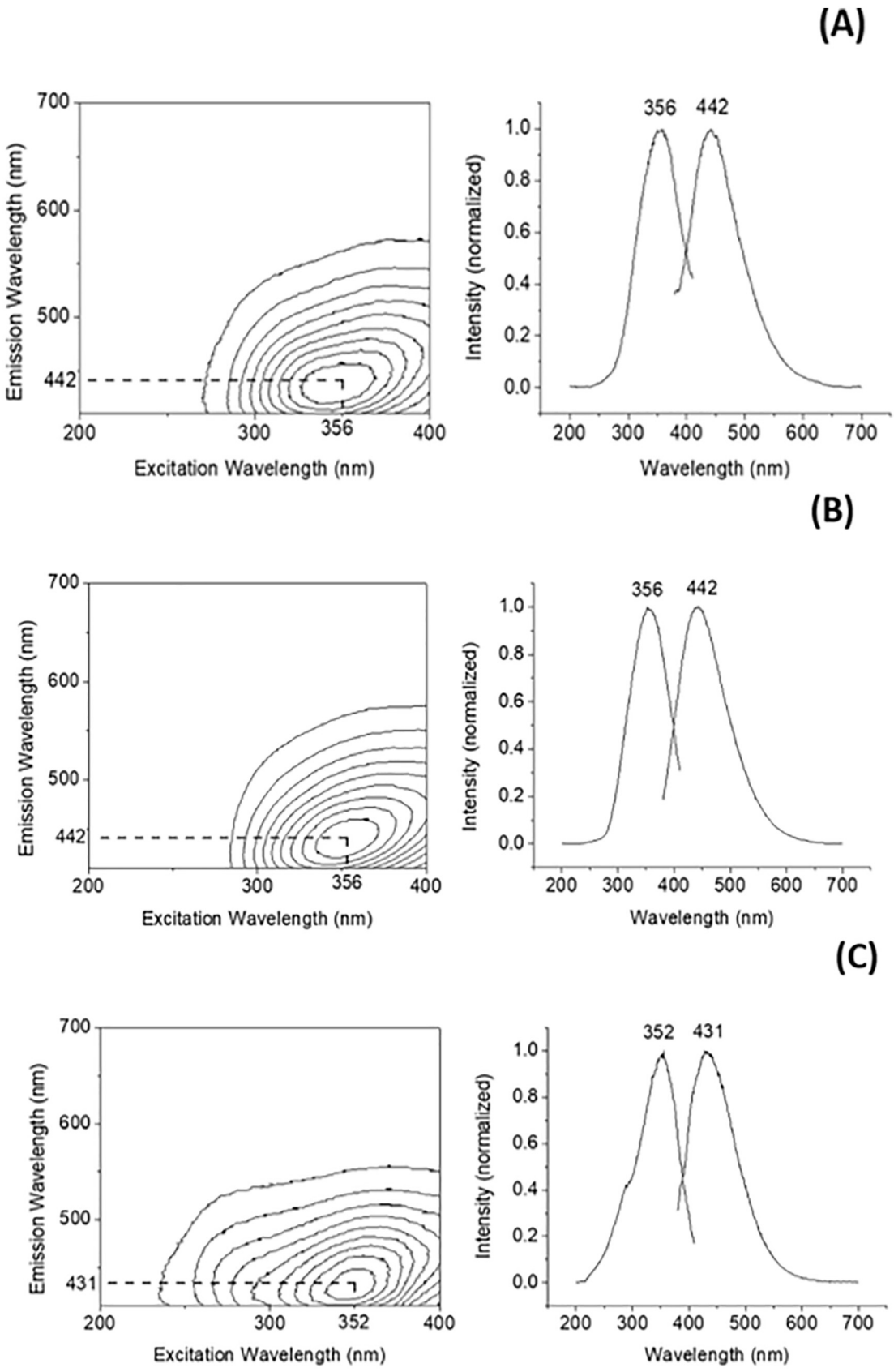

Fig. 1. Fluorescence excitation-emission matrix (EEM) and excitation and fluorescence spectra of the following pre-treated water samples: (A) 06A (B) 07A (C) BWW. Each water sample was pre-filtered with polypropylene filters. Excitation and emission band-pass values were set at 3 nm. EEMs were collected by emission scans from 410 to 700 nm at 1 nm steps with excitation wavelengths from 200 to 400 at 5 nm steps. Excitation and fluorescence spectra were recorded at excitation and emission maxima using 1 nm monochromator steps.

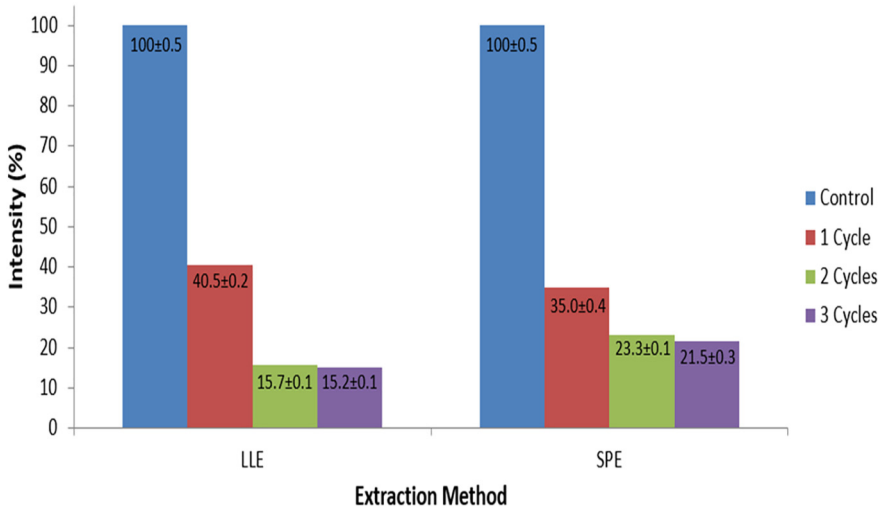

Fig. 2. Relative fluorescence intensities of environmental water sample 07A before and after extraction cycles of LLE or SPE. Each water sample was pre-filtered with polypropylene filters. Each intensity value (in percentage) is the ratio of the average of three intensities over the intensity of the control (no extraction) recorded after independent extractions of three aliquots of water sample.

Based on these results, all further studies were performed with polypropylene filters.

3.7. Lifetime analysis

The luminescence lifetime of the probe ($[Tb\text{-}EDTA]^{-1}$) provides a qualitative parameter for monitoring chemical interference in environmental waters. Previous report investigated the potential interference of inorganic ions often present in urine samples [42]. These included NO_3^-, CH_3COO^-, NO_2^-, OH^-, CO_3^{-2}, I^-, Cl^- and F^-. All the tests were done with ion concentrations at the 10^{-4} mol·L^{-1} level. No interference was observed from NO_3^-, CH_3COO^- and OH^-. While quenching of the luminescence signal was observed in the presence of I^- and NO_2^-, the presence of CO_3^{-2}, Cl^- and F^- caused and enhancement of the luminescence signal of the sensor [42].

Table 2 compares the response of the probe – i.e. 50 μL of a 10^{-4} M Tb-EDTA in 450 μL of 2.5 mM HEPES buffer – in the absence (npH_2O) and the presence of the three inorganic ions (PO_4^{3-}, SO_4^{2-} and Cl^-) known to be present in water samples 06A, 07A and BBW. The ion concentrations were adjusted to mimic the composition of the water samples under investigation. The statistical differences ($\alpha = 0.05$; $N_1 = N_2 = 3$) of the signal intensities of the probe (Tb-EDTA) in the absence and the presence of PO_4^{3-}, SO_4^{2-} and Cl^- suggest potential interference in the analysis of Pi in environmental waters.

Table 3 reports the photoluminescence lifetimes and the signal intensities of the probe (50 μL of a 10^{-4} M Tb-EDTA in 450 μL of 2.5 mM HEPES buffer) in the presence of water samples 06A, 07A and BWW. All the lifetime values are statistically different ($\alpha = 0.05$; $N_1 = N_2 = 3$) to the average lifetime of the probe in 2.5 mM HEPES buffer ($\tau = 1324 \pm 14$ ms). The observed differences are a strong indication of

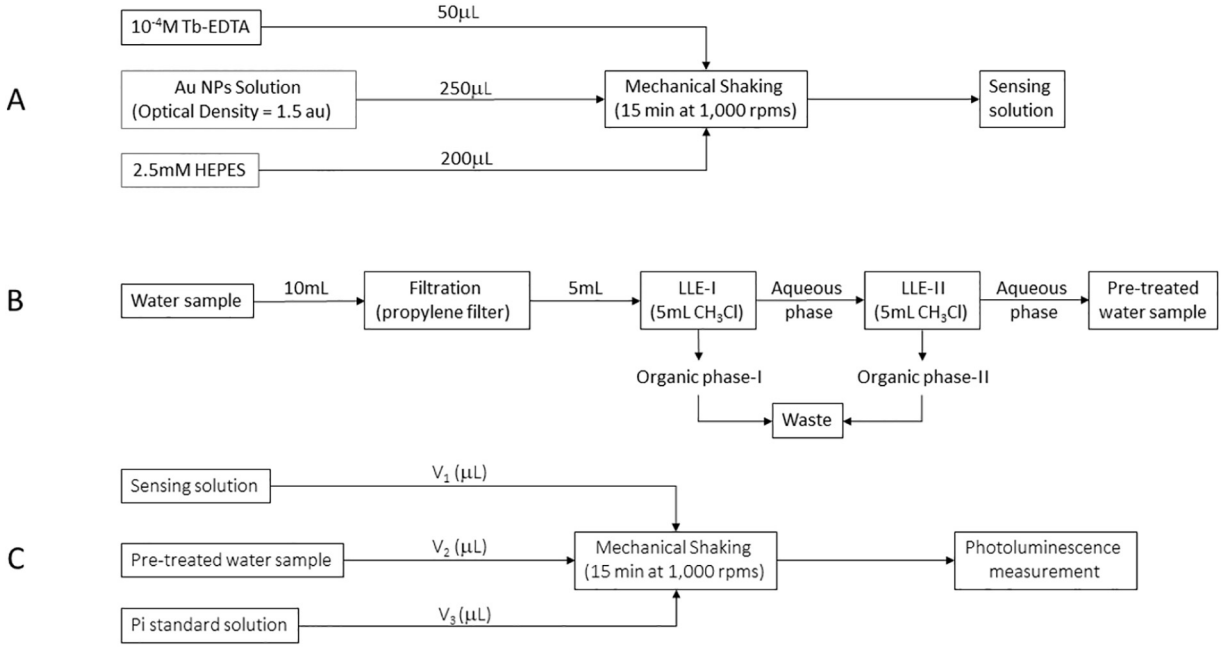

Fig. 3. Experimental procedures for the preparation of sensing solution (A); pre-treatment of water samples (B); and (C) determination of Pi concentrations in environmental water samples. Final volume of the analytical sample (V_{Total}) = 500 μL = $V_1 + V_2 + V_3$; where V_1 = volume of sensing solution, V_2 = volume of water sample; V_3 = volume of Pi standard solution.

chemical interference from the sample matrix, including PO_4^{3-}, SO_4^{2-}, Cl^- and dissolved organic matter (DOM). DOM has a significant effect on metal complexation in aquatic systems. In addition to its potential for chemical interaction with Tb^{3+} interference, DOM absorbs strongly in the ultraviolet and visible regions of the spectrum. Statistical comparison ($\alpha = 0.05$; $N_1 = N_2 = 3$) of the photoluminescence intensity of the probe in the absence (1324 ± 14; $N = 3$) and the presence of environmental waters shows a significant intensity drop that can be attributed to DOM inner filter effects. Similar to PO_4^{3-}, SO_4^{2-} and Cl^-, the presence of DOM in the analytical matrix could lead to inaccurate Pi concentrations.

3.8. LLE and SPE of environmental water samples

Among the photoluminescence techniques we often use to monitor DOM in water samples [51–53], we chose room-temperature fluorescence/excitation-emission matrix (RTF-EEM) spectroscopy [53]. The emission profile of a mixture with numerous fluorescence components varies with the excitation wavelength. EEMs gather this information in a single data format that provides the true signature of the total fluorescence of a sample. EEMs were recorded within 200–350 nm (excitation) and 400–800 nm (emission) using 5 nm and 1 nm monochromator steps, respectively. Scatter interference was avoided with the use

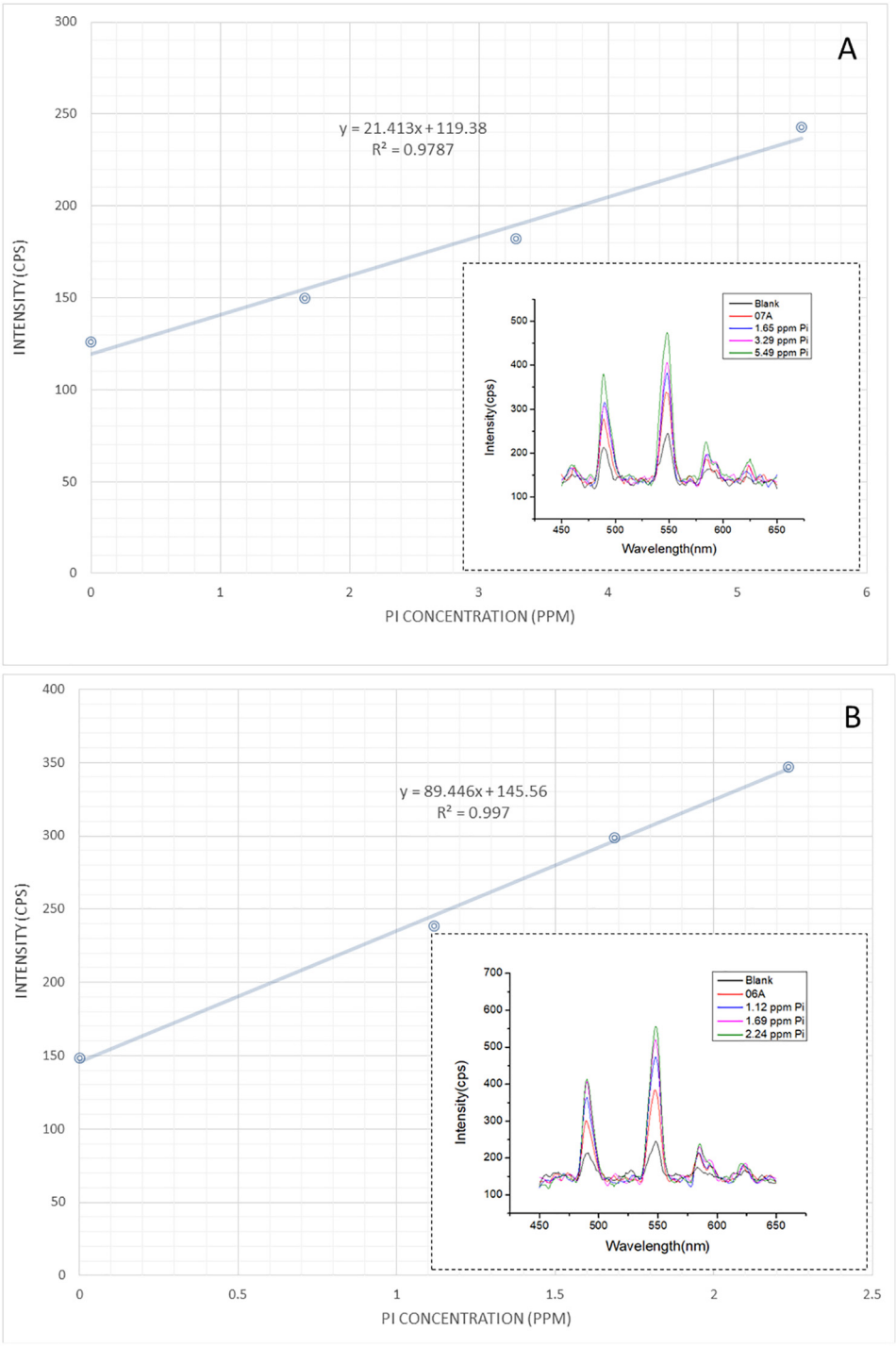

Fig. 4. Multiple standard addition plots obtained with the Pi sensor from the analysis of environmental waters 07 (A), 06A (B) and BWW (C). The spectral indents show the emission response of the sensor upon multiple standard additions. Blank refers to the signal of the sensor in the absence of environmental water.

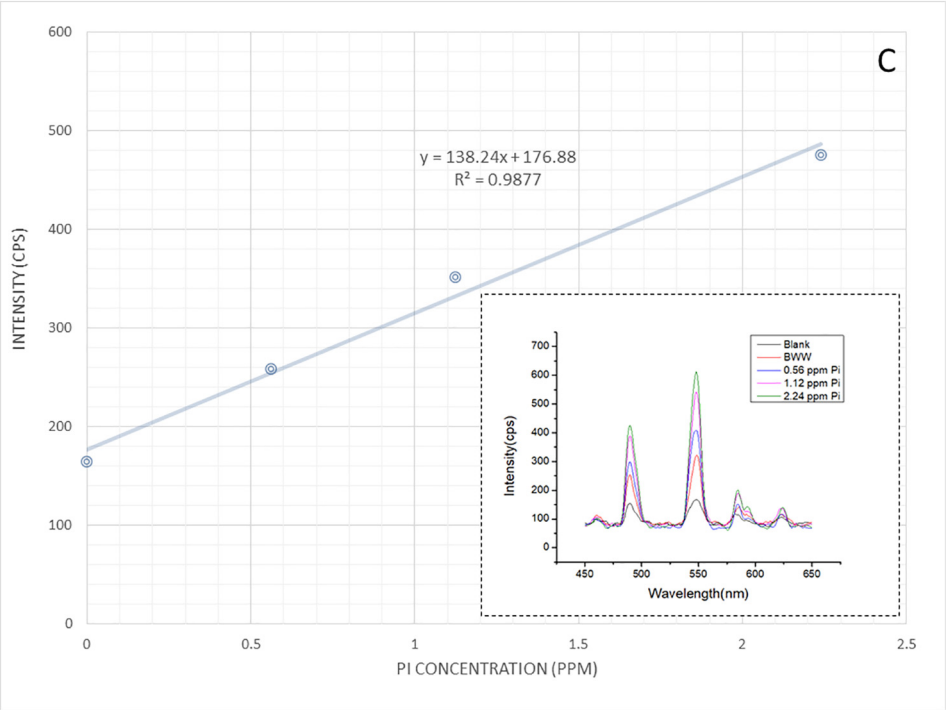

Fig. 4 (*continued*).

of appropriate cut-off filters. As shown in Fig. 1, water 06A, 07A and BWW gave EEMs with maximum intensities at similar excitation and emission wavelengths; namely 356/442 nm (06A and 07A) and 352/431 nm (BWW). Water sample 07A showed a maximum fluorescence intensity approximately three times higher than the maximum fluorescence intensities of water samples 06A and BWW. The extraction efficiencies of the LLE and SPE procedures, therefore, were investigated by monitoring the fluorescence intensity of water sample 07A at its maximum excitation and emission wavelengths.

Fig. 2 summarizes the fluorescence intensities of water sample 07A submitted to three consecutive LLE or SPE cycles. Comparison of signal intensities indicates that the LLE procedure removes a larger fraction of fluorescence concomitants than the SPE procedure. This is probably due to the polar nature of the organic compounds in the water sample. A polar organic solvent such as $CHCl_3$ is probably better than a C-18 sorbent for their extraction. Since no significant improvement was observed after two LLE cycles, all further studies were carried out with filtered water samples submitted to two LLE cycles. As expected, the photoluminescence lifetimes of the sensor in the presence of pre-treated water sample 07A (1295 ± 35 ms) was statistically equivalent ($\alpha = 0.05$; $N_1 = N_2 = 3$) to the lifetime of the sensor in the presence of nanopure water ($\tau = 1303 \pm 40$ ms).

Possible Pi losses due to the LLE procedure were investigated by monitoring the aggregation of Au NPs in Pi standard solutions before and after LLE. An example of the obtained results is shown in Fig. S4. The statistically equivalent ($\alpha = 0.05$; $N_1 = N_2 = 3$) absorbance intensities of Au NPs before and after LLE indicate that $CHCl_3$ does not remove significant amounts of Pi from the standard solution. This observation is in good agreement with the fact that $CHCl_3$ does not form hydrogen bonding with Pi.

3.9. Analysis of water samples

The concentration of Pi in environmental waters was determined via the multiple standard additions (MSA) method. Fig. 3 summarizes the main steps involved in the preparation of the sensing solution (A), pre-treatment of water samples (B) and MSA method (C). Fig. 4 shows the calibration plots obtained for the three analyzed samples. The four data points plotted in each graph include the original sample signal – i.e. no standard addition – and signals recorded from three sample aliquots previously spiked with single standards. All the signals plotted in the MSA graphs were blank subtracted. Blank solutions were prepared with nanopure water following the MSA procedure in Fig. 3C. In all cases, the volume of Pi standards (V_3) used for the multiple additions was 10 μL. The concentrations of Pi standards and the volume of water sample (V_2) were adjusted according to the original signals of the analyzed samples. The volume of sensing solution (V_1) varied with the analyzed sample to provide a 500 μL total volume (V_{Total}) of analytical sample.

Table 4 summarizes the results obtained for the three water samples. The tabulated values obtained with the Pi sensor account for the dilution factors of the studied samples, namely 255 (07A), 75 (06A) and 8.5 (BWW). Their comparison to the concentrations obtained via established methodology shows statistically equivalent results ($\alpha = 0.05$; $N_1 = N_2 = 3$).

4. Conclusion

A sensing approach was developed to detect Pi in water samples at concentration levels that pose a threat to environmental health and safety. The sensing mechanism is based on the FRET that occurs

Table 4
Comparison of Pi concentrations in environmental water samples.

Water sample	Sensor (ppm-Pi)	Established method (ppm Pi)	t_{exp}[a]
06A	122.7 ± 23.2	125.7 ± 8.97	0.209
07A	1422 ± 53.2	1508 ± 12.4	2.727
BWW	10.88 ± 1.23	10.82 ± 0.89	0.068

[a] Experimental value of t calculated from the averages and standard deviations of the concentrations of Pi determined by the sensor or the established method (ion chromatography). $t_{exp} \leq t_{crit} = 2.776$ indicates statistical equivalence of the concentrations determined by the two methods.

between Tb-EDTA (donor) and Au NPs (acceptor). In the presence of Pi, Au NPs aggregate and precipitate out of solution. The aggregation of Au NPs results in the restoration of the Tb-EDTA signal, which correlates to Pi concentration in the matrix of analysis. The relatively long emission decay of the lanthanide ion allows the analyst to time-discriminate the strong fluorescence background often present in environmental water samples. This feature provides the sensor with the ability to detect Pi at the parts-per-billion ($ng \cdot mL^{-1}$) concentration levels. The luminescence lifetime of Tb-EDTA makes possible to interrogate the sensor for potential chemical interference in the sample matrix. This feature becomes particularly relevant for the analysis of environmental waters with high levels of DOM. Although water filtration followed by LLE alleviates the interference of organic matter, quantitative analysis via the calibration curve method is prone to inaccurate results. The alternative for quantitative analysis of heavily contaminated water samples was the MSA method. Despite its well-known limitations [54], the MSA method provided accurate determination of Pi concentrations in three environmental water samples. The simplicity of analysis and the commercial availability of rather inexpensive portable phosphorimeters make the developed sensor an attractive alternative for the on-site monitoring of environmental waters.

Acknowledgements

We thank Lyle Johnson and Florida Spectrum Environmental Services for agricultural water samples, as well as Mark Sees and the Iron Bridge Waste Water Treatment Plant for waste water samples.

Appendix A. Supplementary data

Supplementary data to this article can be found online at https://doi.org/10.1016/j.saa.2019.01.082.

References

[1] M.J. Ascott, D.C. Gooddy, D.J. Lapworth, M.E. Stuart, Sci. Total Environ. 572 (2016) 1534–1542.
[2] O. Technologies, The use of phosphates for potable water treatment, http://orendatech.com/wp-content/uploads/2014/02/Potable-Water-Treatment-phosphates.pdf, Accessed date: 1 June 2017.
[3] A.A. Ansari, G.S. Sarvajeet, G.R. Lanza, R. Walter, Eutrophication of Lakes: Causes, Consquences, and Controls, Springer, New York, 2013.
[4] S.P. Boeykens, M.N. Piol, L. Samudio Legal, A.B. Saralegui, C. Vazquez, J. Environ. Manag. 203 (2017) 888–895.
[5] S. Kaur, I. Singh, Int. J. Plant Anim. Environ. Sci. 2 (3) (2012) 183–187.
[6] J.J. Elser, M.E. Bracken, E.E. Cleland, D.S. Gruner, W.S. Harpole, H. Hillebrand, J.T. Ngai, E.W. Seabloom, J.B. Shurin, J.E. Smith, Ecol. Lett. 10 (12) (2007) 1135–1142.
[7] M. Sondergaard, J.P. Jensen, E. Jeppesen, Hydrobiologia 408 (409) (1999) 145–152.
[8] D. Guest, The Massive Fish Kill in Florida Could Have Been Prevented Earthjustice, 2016.
[9] J. Murphy, J.P. Riley, Anal. Chim. Acta 27 (1962) 31–36.
[10] T. Kaur, A. Ganguli, M. Ghosh, Water Sci. Technol. 68 (12) (2013) 2619–2625.
[11] S. Asaoka, Y. Kiso, T. Oomori, H. Okamura, T. Yamada, M. Nagai, Chem. Geol. 380 (2014) 41–47.
[12] O.A. Zaporozhets, L.S. Zin'ko, I.A. Kachan, J. Anal. Chem. 62 (12) (2007) 1146–1150.
[13] N. Gissawong, S. Sansuk, S. Srijaranai, Spectrochim. Acta A Mol. Biomol. Spectrosc. 173 (2017) 994–1000.
[14] A. Afkhami, R. Norooz-Asl, J. Hazard. Mater. 167 (1–3) (2009) 752–755.
[15] S. Motomizu, T. Wakimoto, K. Toei, Talanta 31 (4) (1984) 235–240.
[16] A. Sabarudin, M. Oshima, S. Motomizu, Anal. Chim. Acta 481 (2) (2003) 311–319.
[17] J. Jonica, V. Leon Fernandez, D. Thouron, A. Paulmier, M. Graco, V. Garcon, Talanta 87 (2011) 161–167.
[18] D. Talarico, F. Arduini, A. Amine, I. Cacciotti, D. Moscone, G. Palleschi, Anal. Bioanal. Chem. 408 (26) (2016) 7299–7309.
[19] D. Xiao, H.Y. Yuan, J. Li, R. Yu, J. Anal. Chem. 67 (1995) 288–291.
[20] Y. Bai, J. Tong, C. Bian, G. Yan, B. Deng, H. Zhang, S. Xia, Micro Nano Lett. 7 (12) (2012) 1176–1179.
[21] Y. Bai, Y. Li, S. Xia, J. Sun, C. Bian, J. Tong, Micro Nano Lett. 9 (12) (2014) 862–865.
[22] Y. Li, T. Jiang, X. Yu, H. Yang, J. Electrochem. Soc. 163 (9) (2016) B479–B484.
[23] M. Neves, M. Souto, I. Toth, S. Victal, M. Drumond, A. Rangel, Talanta 77 (2) (2008) 527–532.
[24] H. Haraguchi, K. Masaaki, M. Masatoshi, M. Akira, F. Keiichiro, F. Naoki, Technical Series of Instrumental Analysis: ICP-ES Analysis, Kyoritsu Shuppan Company, Tokyo, 1981.
[25] Z. Guo, Q. Cai, Z. Yang, J. Chromatogr. 1100 (2) (2005) 160–167.
[26] L. Yang, E. Pagliano, Z. Mester, Anal. Chem. 86 (6) (2014) 3222–3226.
[27] S.M. Ng, Trends Environ. Anal. Chem. 3–4 (2014) 36–42.
[28] J. Ye, R.F. Bogale, Y. Shi, Y. Chen, X. Liu, S. Zhang, Y. Yang, J. Zhao, G. Ning, Chemistry 23 (32) (2017) 7657–7662.
[29] Y. Song, Y. Li, Y. Liu, X. Su, Q. Ma, Talanta 144 (2015) 680–685.
[30] D. Zhao, X. Wan, H. Song, L. Hao, Y. Su, Y. Lv, Sensors Actuators B Chem. 197 (2014) 50–57.
[31] M.A. Saeed, D.R. Powell, M.A. Hossain, Tetrahedron Lett. 51 (37) (2010) 4904–4907.
[32] H. Nakamura, K. Ikebukuro, S. McNiven, I. Karube, H. Yamamoto, K. Hayashi, M. Suzuki, I. Kubo, Biosens. Bioelectron. 12 (1997) 959–966.
[33] C.M. McGraw, S.E. Stitzel, J. Cleary, C. Slater, D. Diamond, Talanta 71 (3) (2007) 1180–1185.
[34] H. Xu, C.S. Cao, B. Zhao, Chem. Commun. (Camb.) 51 (51) (2015) 10280–10283.
[35] X. Song, Y. Ma, X. Ge, H. Zhou, G. Wang, H. Zhang, X. Tang, Y. Zhang, RSC Adv. 7 (14) (2017) 8661–8669.
[36] H. Cao, Z. Chen, Y. Huang, Talanta 143 (2015) 450–456.
[37] J. Chen, F.-Y. Yi, H. Yu, X. Liu, L. Han, G. Pang, Eur. J. Inorg. Chem. 2016 (25) (2016) 3994–3998.
[38] M. Turel, A. Duerkop, A. Yegorova, A. Karasyov, Y. Scripinets, A. Lobnik, Anal. Chim. Acta 675 (1) (2010) 42–48.
[39] M. Swierczewska, S. Lee, X. Chen, Phys. Chem. Chem. Phys. 13 (21) (2011) 9929–9941.
[40] J. Homola, Chem. Rev. 108 (2008) 462–493.
[41] M.-C. Daniel, D. Astruc, Chem. Rev. 104 (2004) 293–346.
[42] A.A. Fadhel, M. Johnson, K. Trieu, E. Koculi, A.D. Campiglia, Talanta 164 (2017) 209–215.
[43] M. Santos, B.C. Roy, H. Goicoechea, A.D. Campiglia, J. Am. Chem. Soc. 126 (2004) 10738–10745.
[44] B. Nikoobakht, M.A. El-Sayed, Chem. Mater. 15 (10) (2003) 1957–1962.
[45] S.Y. Moon, T. Kusunose, T. Sekino, Mater. Lett. 63 (23) (2009) 2038–2040.
[46] B.C. Roy, M. Santos, S. Mallik, A.D. Campiglia, J. Org. Chem. 68 (2003) 3999–4007.
[47] H. Goicoechea, B.C. Roy, M. Santos, A.D. Campiglia, S. Mallik, Anal. Biochem. 336 (1) (2005) 64–74.
[48] S.L. Wu, W.D. Horrocks Jr., Anal. Chem. 68 (1996) 394.
[49] S. Zhuo, L. Chen, Y. Zhang, G. Jin, Spectrosc. Lett. 49 (1) (2016) 1–4.
[50] S.J. Xiao, X.J. Zhao, J. Zuo, H.Q. Huang, H. Zhang, Anal. Chim. Acta 906 (2016) 148–155.
[51] J.L. Whitcomb, A.J. Brystol, A.D. Campiglia, Anal. Chim. Acta 464 (2) (2002) 261–272.
[52] A.D. Campiglia, T. Vo-Dinh, Talanta 43 (10) (1996) 1805–1814.
[53] A.F.T. Moore, H.C. Goicoechea, F. Barbosa Jr., A.D. Campiglia, Anal. Chem. 87 (10) (2015) 5232–5239.
[54] M. Thompson, AMC Technical Briefs No 37, 1757-5958, March 2009.